Particle motion on burned and vegetated hillslopes

Danica L. Roth[a,1], Tyler H. Doane[b], Joshua J. Roering[c], David J. Furbish[d,e], and Aaron Zettler-Mann[f]

[a]Department of Geology and Geological Engineering, Colorado School of Mines, Golden, CO 80401; [b]Department of Earth and Atmospheric Sciences, Indiana University, Bloomington, IN 47405; [c]Department of Earth Sciences, University of Oregon, Eugene, OR 97403; [d]Department of Earth and Environmental Sciences, Vanderbilt University, Nashville, TN 37235; [e]Department of Civil and Environmental Engineering, Vanderbilt University, Nashville, TN 37235; and [f]Department of Geography, University of Oregon, Eugene, OR 97403

Edited by Douglas W. Burbank, University of California, Santa Barbara, CA, and approved August 31, 2020 (received for review December 20, 2019)

Climate change is causing increasingly widespread, frequent, and intense wildfires across the western United States. Many geomorphic effects of wildfire are relatively well studied, yet sediment transport models remain unable to account for the rapid transport of sediment released from behind incinerated vegetation, which can fuel catastrophic debris flows. This oversight reflects the fundamental inability of local, continuum-based models to capture the long-distance particle motions characteristic of steeplands. Probabilistic, particle-based nonlocal models may address this deficiency, but empirical data are needed to constrain their representation of particle motion in real landscapes. Here we present data from field experiments validating a generalized Lomax model for particle travel distance distributions. The model parameters provide a physically intuitive mathematical framework for describing the transition from light- to heavy-tailed distributions along a continuum of behavior as particle size increases and slopes get steeper and/or smoother. We show that burned slopes are measurably smoother than vegetated slopes, leading to 1) lower rates of experimental particle disentrainment and 2) runaway motion that produces the heavy-tailed travel distances often associated with nonlocal transport. Our results reveal that surface roughness is a key control on steepland sediment transport, particularly after wildfire when smoother surfaces may result in the preferential delivery of coarse material to channel networks that initiate debris flows. By providing a first-order framework relating the statistics of particle motion to measurable surface characteristics, the Lomax model both advances the development of nonlocal sediment transport theory and reveals insights on hillslope transport mechanics.

sediment transport | dry ravel | postfire erosion | nonlocal transport | roughness

Wildfire frequency in the western United States has increased drastically (1) in recent decades. Forecasted changes in climate (2) indicate that prolonged drought conditions and intensifying winter storms on the West Coast will continue to increase wildfire occurrence and associated hazards in the coming years (3). Particularly concerning is the growing hazard of postwildfire hazards such as debris flows. Recent work suggests that some debris flows may be fueled (4–9) by sediment trapped or stabilized behind vegetation and released to travel long distances via dry ravel after wildfire (4, 6, 10–14). The majority of this mobilization occurs rapidly. At our study site in the Oregon Coast Range (OCR), for example, 2/3 of erosion in the first year after wildfire may occur in just the first 24 h (15). Postfire erosion exceeds long-term erosion rates by a factor of 6 (12) in the OCR and up to a factor of 30 (16) in the chaparral steeplands of Southern California, accounting for ∼25 to 70% of long-term sediment yield (12, 16). Dry ravel is thought to be a primary postfire erosional process in many steep landscapes (6, 12–14, 17, 18). Some work has been done to develop explicit, particle-based physical models for postfire dry ravel (11, 19–21). Yet general formulae for geomorphic transport remain unable to account for the fluxes of such sediment, or to predict how debris flow hazards and whole landscapes may evolve as fires and fire-induced transport events increase in frequency or magnitude (1–3).

In fact, this problem highlights the more basic inability of hillslope sediment transport models to account for long-distance particle motion over variable topography. This inability represents a knowledge gap in our capacity to predict sediment transport and landscape dynamics not only after wildfires but in any steepland setting. As much of the active transport on Earth—especially high-magnitude events and responses to perturbation like wildfire—involves steepland processes (14), this gap currently hampers progress on a wide range of geomorphology, land management, hazard mitigation, and other topics.

Commonly used hillslope sediment transport models (22–24) represent time-averaged or spatially averaged sediment fluxes under the assumptions (25) that fluxes 1) can be characterized without accounting for individual particle movements and 2) are calculable entirely from "local" characteristics at a given position (e.g., slope, soil thickness). For soil creep processes in which the soil column approximates a continuum undergoing internal biomechanical disturbances in concert with granular creep (26–28), these assumptions are generally (23, 29–35) [although not completely (27, 36, 37)] defensible. However, local models are entirely unable to account for inertia-based particle motion that initiates far upslope and traverses the surface rather than being constrained by the soil column. In steep environments, processes like rock fall (38) and dry ravel (13, 14, 20, 39) can generate particle movement that traverses the surface over distances approaching the scale of topographic variations or the hillslope itself. These processes are often precipitated by disturbances like wildfires (4, 10–12), tree throw (40), and burrowing animals (41),

Significance

Commonly used sediment transport models are fundamentally unable to account for long-distance particle motions characteristic of steep regions. This type of transport is a primary cause of elevated erosion rates after wildfire and may even contribute to postfire debris flows in some areas. Here we show that the incineration of vegetation causes measurable changes in surface roughness that drastically increase particle travel distances. Our data demonstrate that long-distance particle motion falls into three distinct regimes along a continuum that can be systematically represented by a simple model that scales with surface slope, roughness, and particle size. These results represent a key first-order step toward accounting for the effects of surface roughness on long-distance transport when predicting postfire and steepland erosion.

Author contributions: D.L.R., J.J.R., and D.J.F. designed research; D.L.R., T.H.D., and J.J.R. performed research; A.Z.-M. collected and processed photogrammetric data; D.L.R. analyzed data; D.L.R. wrote the paper; and T.H.D., J.J.R., and D.J.F. provided discussion and input on paper.

The authors declare no competing interest.

This article is a PNAS Direct Submission.

[1]To whom correspondence may be addressed. Email: droth@mines.edu.

This article contains supporting information online at https://www.pnas.org/lookup/suppl/doi:10.1073/pnas.1922495117/-/DCSupplemental.

which are stochastic and patchy due to thin soil mantling, bedrock exposure (42), and other forms of heterogeneity common in steeplands. As particle travel distances increase, the sediment flux at a given position is increasingly influenced by particle interactions with upslope or "nonlocal" topography (43, 44). Time-averaged and spatially averaged local formulations provide wholly inadequate descriptions of such particle motion (25), which can be better represented by probabilistic and particle-based descriptions (20, 25, 39, 43–50).

In order to account for long-distance motions, recent formulations (43, 44, 50) describe the sediment flux at a given position through a convolution of upslope conditions that influence any particle motions reaching that position. Here we focus on a scale-invariant, probabilistic formulation (43, 44) that expresses the sediment flux explicitly in terms of the distribution of particle travel distances. The flux at any position can be obtained by convolving the volumetric rate of sediment entrained upslope with the travel distance exceedance probability (i.e., proportion of entrained sediment that exceeds a given distance, or the complementary cumulative distribution function of travel distances) for all upslope positions (43, 44). More simply, the flux at any position is the sum of all sediment that is entrained upslope and that does not become disentrained before reaching that position. This formulation provides a flexible yet mathematically robust framework for assessing long-distance sediment transport over any surface using physical parameters that are well defined and accessible, for instance, through high-resolution topographic data.

However, the connections between the statistics of particle motion and the physical parameters that control them lack clarity. Previous theoretical advances to nonlocal transport theory have therefore focused either on grain-scale models of particle motion (20, 25, 39, 45) built on simplified physics or on probabilistic (43, 44, 51, 52) or analytical (49, 50) solutions for hillslope profiles that rely on assumed particle entrainment rates and travel distance distributions. Recent work on hillslope particle entrainment has centered on formalizing a time-averaged definition (52), while others have considered it indirectly (10, 11, 53, 54), and this subject merits further consideration. Particle disentrainment, however, remains almost entirely unstudied on hillslopes. To our knowledge, no previous studies have directly examined hillslope particle disentrainment, although it fundamentally regulates the distances particles travel (*SI Appendix*, Eq. **S1**). As disentrainment is, in turn, governed by the physics of particle–surface, and, in some cases, particle–particle, interactions, it provides an appealing framework for linking physically based rules to the distribution of particle travel distances. Here we examine particle–surface interactions with an explicit focus on disentrainment and its relation to particle travel distance distributions.

Laboratory and field studies have been inconclusive regarding the forms of these distributions, but some suggest (20, 39, 45, 55) they may be exponential or light-tailed for small particles or at low slopes, and that average travel distances increase and distributions may become heavy tailed at higher slopes or as particle sizes increase relative to surface roughness. These influences have not been systematically quantified or documented in the context of naturally occurring variations in surface roughness or topography. To address this gap, we developed a first-order model for the systematic influence of these physical controls on particle travel distance distributions in natural settings, which we tested through rock drop experiments on burned and forested hillslopes in the OCR (Fig. 1). This model provides a mathematically simple yet empirically consistent framework for describing a natural transition from light- to heavy-tailed travel distances in relation to the physical factors that control particle motions and disentrainment, namely, surface slope, roughness, and particle size.

We conducted rock drop experiments with three grain sizes across a range of surfaces and gradients ($S = 0.25$ to 0.81) in the OCR (*SI Appendix*, Fig. S1): Four hillslopes were vegetated with dense, old-growth forest, while three slopes had lost all vegetation in a high-severity burn ~1 mo prior (Horse Prairie wildfire, summer 2017). At each site, we assessed a median surface roughness height d_{50} using detrended and Gaussian-filtered digital elevation data (Fig. 2) measured with either terrestrial lidar or photogrammetry. More details about the sites, rock drop experiments and topographic data collection, processing, and analysis are available in *SI Appendix*, sections 1 and 2 and Tables S1 and S2. Surface roughness is more varied and up to an order of magnitude larger on forested slopes ($d_{50} = 0.02$ m to 0.12 m) than on burned slopes ($d_{50} = 0.016$ m to 0.019 m). Assuming similar preexisting conditions, this is a measurable demonstration of wildfire's effectiveness at removing surface roughness, which creates an optimal natural laboratory for isolating and exploring the consequences of varying roughness on particle motion. Our initial results demonstrate that particles generally travel farther on burned slopes and tend to collect near obstacles like roots and trees on the vegetated slopes (Fig. 2 and *SI Appendix*, Fig. S2).

We calculate the empirical exceedance probability of particle travel distances $R(x)$ (dimensionless) and the spatial rate of particle disentrainment $P(x)$ (per unit length) from the travel distances measured for each experimental slope and grain size combination (*SI Appendix*, section 3). We model our observed $R(x)$ and $P(x)$ with a Lomax distribution (i.e., generalized Pareto with location parameter of 0) jointly optimized for $R(x)$ (Figs. 3–5 and *SI Appendix*, section 4),

$$R_{model}(x) = \begin{cases} \left(\frac{Ax}{B} + 1\right)^{-1/A} & for\ A \neq 0 \\ exp\left(-\frac{x}{B}\right) & for\ A = 0 \end{cases} \quad [1]$$

and

$$P_{model}(x) = \frac{1}{Ax + B}, \quad [2]$$

where A (dimensionless) is a shape parameter and B (length) is a scale parameter.

We chose the Lomax distribution (Eq. **1**) due to its ability to represent the progression of travel distance distributions from light tailed ($A < 0$) through exponential ($A = 0$) to heavy tailed ($A > 0$). As illustrated in the conceptual diagram in Fig. 3, this transition in tail behavior is caused by a shift from spatially increasing to spatially decreasing particle disentrainment, which, respectively, denote what we will call "bounded" and "runaway" states of particle motion occurring at a characteristic travel

Fig. 1. (*A*) Experimental locations in Oregon (○ = burned, △ = vegetated; see *SI Appendix*, Table S2 for all site coordinates) and (*B* and *C*) example field photos showing experimental setup and site characteristics for burned ($S = 0.31$) and vegetated ($S = 0.81$) hillslopes.

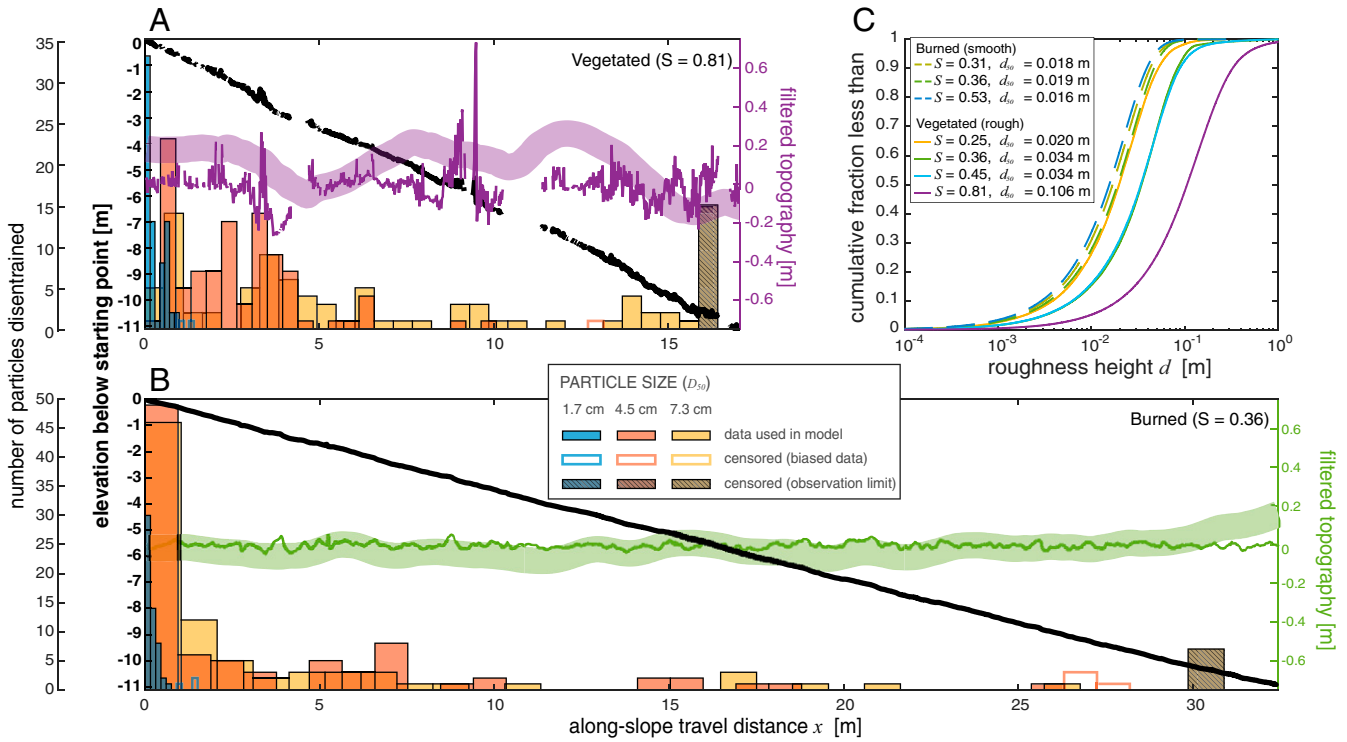

Fig. 2. Example hillslope profiles (black lines) and particle travel distance histograms (shown on matching scales) for (*A*) vegetated ($S = 0.81$) and (*B*) burned ($S = 0.36$) hillslopes. For each transect, long-wavelength Gaussian-filtered topography (thick colored lines) represents surface-normal variations about the mean hillslope plane over distances $\gtrsim 1$ m, while short-wavelength topography (thin colored lines) captures smaller variations about that long-wavelength surface over distances $\lesssim 1$ m. Histograms include all recorded data, including data censored due to surpassing the limit of observations and due to biasing Lomax fits by overweighting the distribution tails. (*C*) Cumulative distributions of roughness height *d* for all experimental slopes *S*, as well as corresponding median value d_{50} used as a metric for surface roughness. Note that the 0.25-gradient vegetated slope is nearly as smooth as the burned slopes. See *SI Appendix*, section 1 for details on topographic data filtering and roughness analysis techniques.

distance $B/|A|$. Particle motion over smaller scales is described by B, which scales inversely with the initial particle disentrainment rate $P_{model}(0) = 1/B$ near $x = 0$. B also represents the mean particle travel distance if the distribution is exponential. The Lomax parameters therefore provide an intuitive yet quantitatively rigorous framework for describing how physical factors dictate particle behavior across all scales along the light- to heavy-tailed progression.

We find that observed particle travel distance exceedance probabilities $R(x)$ and particle disentrainment rates $P(x)$ are well represented by this Lomax distribution model (Fig. 4). Indeed, our observed $P(x)$ and $R(x)$ (shown in Fig. 5) clearly demonstrate both the patterns described in Fig. 3 and their dependence on physical factors. Smaller clasts on lower-gradient or rougher slopes have lower B values, reflecting their higher likelihood of disentrainment relative to larger clasts on steeper or smoother slopes (Fig. 5). Our experimental distributions clearly demonstrate the progressive transition from light- to heavy-tailed as experimental slope or particle size increases (Fig. 5), particularly in the absence of surface roughness on the burned slopes.

These behaviors result from the balance in energy gained and lost by particles as they travel, represented by the ratio SD_{50}/d_{50} (Fig. 6). Slope S represents the spatial rate of conversion from potential to kinetic energy as particles travel downhill, while d_{50}/D_{50}, also known as relative roughness (20, 39, 45, 56), is assumed to measure the effectiveness with which the surface extracts kinetic energy from mobile grains of a given size. Hence, small grains lose more energy and are more likely to disentrain while traveling on low slopes with higher surface roughness. Conversely, larger grains on steeper or smoother slopes retain or gain more kinetic energy as they travel, making disentrainment less likely. As SD_{50}/d_{50} increases, particles with light-tailed distributions ($A < 0$) are thus able to travel increasingly longer distances before their motion is bounded ($B/|A|$ increases and tails grow less light; highlighted with blue clusters in Fig. 6 *A* and *C*). Distribution tails eventually transition to heavy tailed ($A > 0$), indicating a shift to runaway particle motion, which occurs at decreasing distances ($B/|A|$ declines and distribution tails grow increasingly heavy; highlighted with green clusters in Fig. 6 *A* and *C*) with further increases in SD_{50}/d_{50}.

While we are unable to fully isolate and examine the effects of roughness, because d_{50} covaries with slope ($r = 0.84$), the contrast in Lomax parameters and travel distances at the vegetated and burned slopes with matching gradients ($S = 0.36$) provides a compelling demonstration of its impact (Fig. 5 and *SI Appendix*, Fig. S2). We also plot $B/|A|$ against SD_{50} in Fig. 6 *B*, *D*, and *F* to compare the variance in these parameters without accounting for roughness. We see a clear separation between the smooth and rough datasets and the same systematic variation over positive and negative A values for the data from each individual slope of a given roughness. Normalizing by d_{50} shifts the outlying light-tailed ($A < 0$) and heavy-tailed ($A > 0$) data more into alignment. This also notably shifts the approximate transition from negative to positive A values closer to $SD_{50}/d_{50} = 1$, where we expect the theoretical balance in energy gained and lost to produce exponential distributions ($A = 0$ and $B/|A| \to \infty$). These findings are consistent with the premise that roughness contributes a majority of the remaining variance between $B/|A|$ or A and SD_{50}. In contrast, variance in parameter B is better minimized by

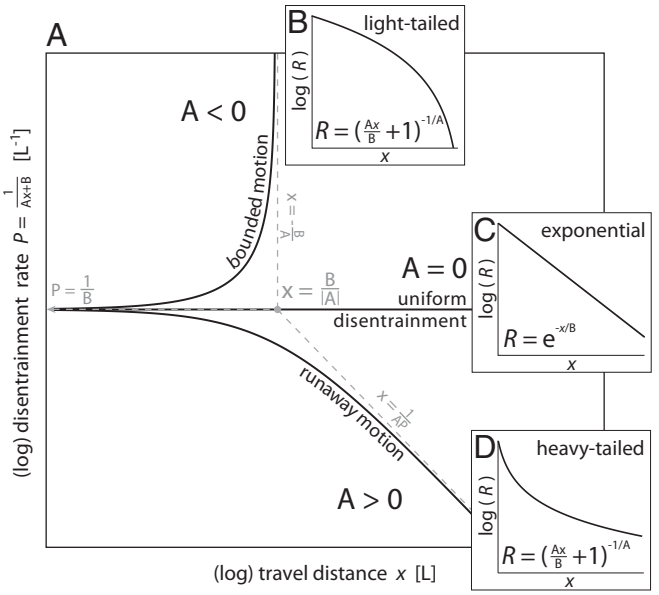

Fig. 3. Cartoon demonstrating Lomax representation of particle disentrainment $P(x)$ behavior and associated travel distance exceedance distributions $R(x)$. (*A*) Disentrainment is approximately uniform ($P \sim 1/B$) over small travel distances near $x \sim 0$. Over longer travel distances, disentrainment behavior and distribution tails fall into three distinct categories reflected in Lomax parameter *A*. (*B*) For $A < 0$, particles experience bounded motion, becoming increasingly likely to stop as they approach an asymptote at $x = B/|A|$, which leads to light-tailed travel distance distributions (concave down in semilog space). As negative *A* values approach zero, $B/|A|$ increases and motion becomes bounded at longer distances, approaching (*C*) uniform disentrainment $P = 1/B$ and exponential distributions (straight line) at $A = 0$ or $B/|A| = \infty$. (*D*) As *A* continues to increase ($A > 0$), disentrainment begins to decline with distance, making particles increasingly less likely to stop as they travel farther and producing heavy-tailed distributions (concave up). This runaway motion is controlled by an oblique asymptote $x = 1/AP$ that intersects with $P = 1/B$ at $x = B/|A|$. As positive *A* values grow larger and $B/|A|$ decreases, particles experience runaway motion at shorter distances, and the distribution's tail grows increasingly heavy. See Fig. 2 for observations of each behavior.

scaling with SD_{50} than SD_{50}/d_{50} (Fig. 6 *E* and *F*), consistent with $B \sim 1/P(0)$ representing initial disentrainment over short scales before particles encounter much roughness. Combined, these findings demonstrate the Lomax distribution model's basic fidelity to the physics of particle motion. Therefore, while the correlation between $B/|A|$ and SD_{50}/d_{50} is stronger over $A > 0$ than over $A < 0$ (Fig. 6*A*; $r_+ = -0.79$; $r_- = 0.61$), we suspect this simply reflects (57) both the scarcity of data for $A < 0$ and the insufficiency of *A*, *B*, and SD_{50}/d_{50} to fully represent the physics of particle–surface interactions. For example, this representation does not account for the full distribution of surface roughness or experimental particle sizes; particle shape; the spatial frequencies of roughness elements; small-scale slope variations; nonlinearities in the dependence of $B/|A|$ on *S*, D_{50}, or d_{50}; or any fire-induced changes in the elastomechanical properties of the hillslope surface.

We also note that, while the 0.25-gradient vegetated slope was materially identical to the other vegetated slopes (*SI Appendix*, Fig. S1*D*), its Lomax parameters are consistent with the burned slopes (Fig. 6) it more closely resembled in roughness (Fig. 2). Further, the two larger particle size classes experienced runaway motion at this site despite its gradient being the lowest of all experimental slopes and its measured particle travel distances being the shortest (consistent with high initial disentrainment, i.e., low Lomax parameter *B*). Travel distances on the steeper vegetated slopes were far longer, and initial disentrainment was lower, yet runaway motion did not occur until a gradient of 0.81. Even at this extreme slope, only the largest particles demonstrated a heavy-tailed Lomax parameter of $A = 0.35$, compared to $A = 0.64$ and 1.18 (medium and large particles, respectively) at the smooth, lowest slope (Fig. 5). These observations indicate that roughness plays a dominant role in controlling the forms of particle travel distance distributions.

Disentrainment on Inhomogeneous and Evolving Natural Surfaces

On an idealized hillslope on which the physical properties controlling particle disentrainment (i.e., *S*, D_{50}, and d_{50}) remain constant in both time and space, we expect the movement of a large number of identical particles to be perfectly represented by a single pair of *A* and *B* values. In a natural landscape, however, these physical properties may be neither steady nor uniform. Surface roughness, topography, and mobile grain sizes can systematically vary with position [e.g., talus slopes (39, 56, 58) and deltas (59) commonly exhibit downslope surface coarsening], and evolve over timescales both long (e.g., under tectonic or climatic forcing) and short (e.g., as vegetation regrows after wildfire). Our data (Fig. 5) demonstrate that variation in surface properties produces distinct variation in particle disentrainment and travel distance distributions over space, and—if we imagine the burned and vegetated sites as endmember states in the cyclical growth and loss of surface roughness to wildfire—over time. The large bumps in *R* where particles experienced high localized rates of disentrainment tend to correspond to the positions of large roots and trees on the vegetated slopes and small variations in long-wavelength surface gradient on the burned slopes (Fig. 2 and *SI Appendix*, Fig. S2). These locally high disentrainment rates underscore the probabilistic arrangement of roughness elements and hence the probabilistic nature of particle motion along a rough hillslope. The variation we observe in *R* and *P* (Fig. 5) could be viewed as a series of brief intervals of bounded or runaway motion that are quickly stalled or reversed by spatially variable surface conditions. A Lomax distribution optimized over the entire hillslope, such as the *A* and *B* values we optimized for each sample distribution, therefore captures the hillslope-averaged impact of these spatially variable conditions, which may be represented to first order by the average grain size, surface slope, and roughness (Fig. 6). While we present a simple inverse model, this insight suggests that a physically informed forward model might enable the characterization of spatially and temporally averaged conditions controlling long-term particle motion under steady and uniform conditions.

For a more complete treatment of the details of particle motion and the physics of particle–surface interactions, the distributions and variations in grain size, surface roughness, and topography (as well as other variables such as initial particle kinetic energy, elastomechanical properties, and particle shape)

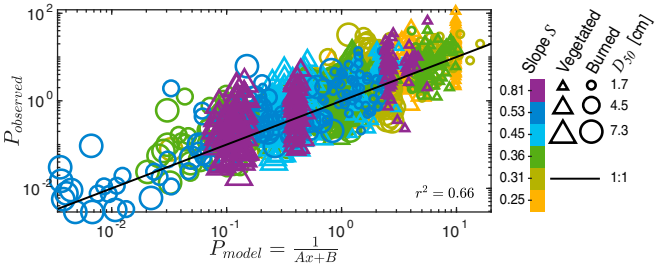

Fig. 4. Observed and modeled particle disentrainment rate *P* for all data. Lomax distribution parameters *A* and *B* were fit by joint optimization to *R* values observed for each experimental combination of grain size D_{50} and slope *S*.

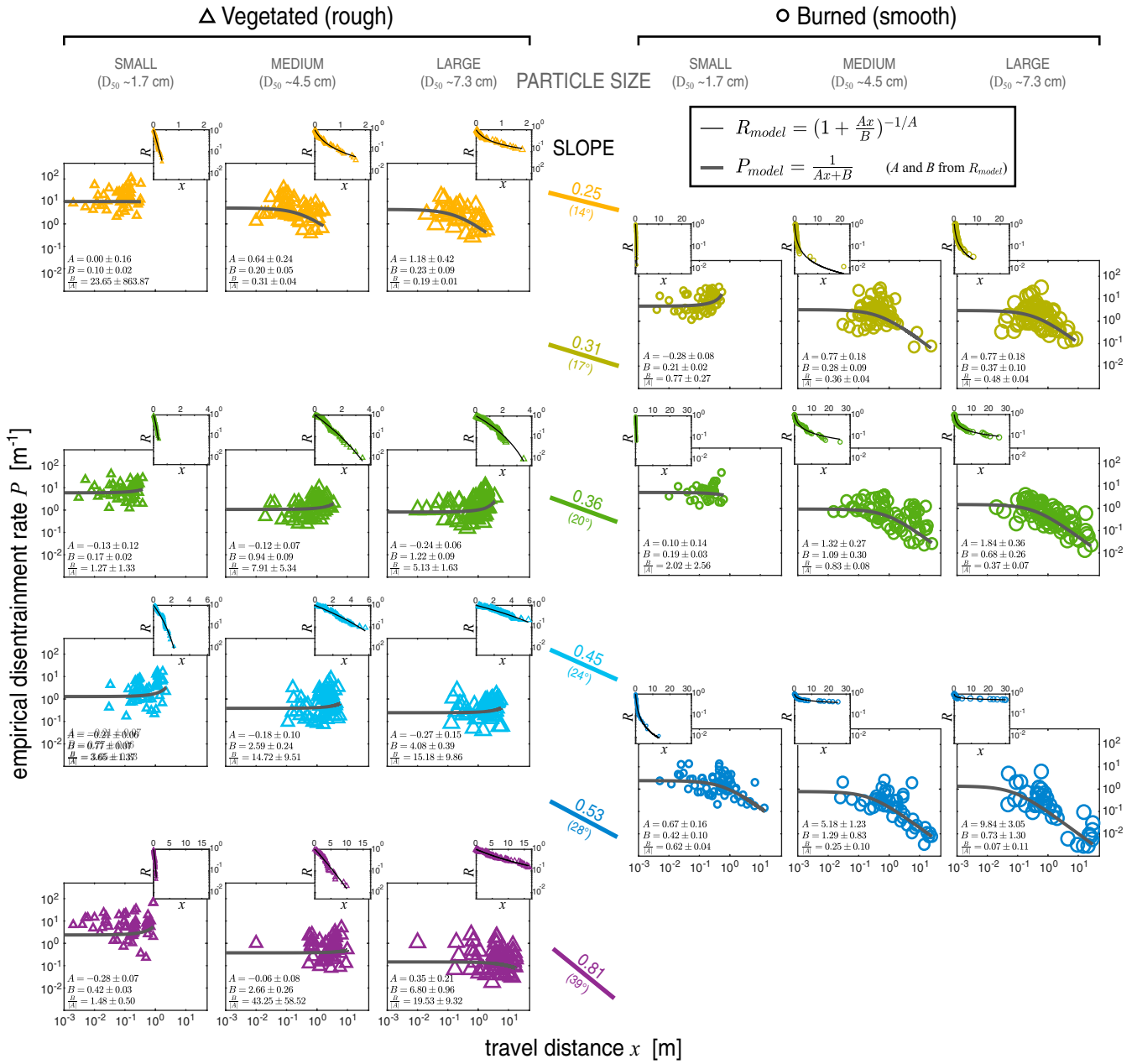

Fig. 5. Empirical spatial disentrainment rate P as a function of particle travel distance x, with travel distance exceedance probability distributions R shown as *Insets* for each experimental slope (increasing downward) and particle size (increasing toward the right) on vegetated (*Left*) and burned (*Right*) hillslopes. Surface slopes are reported as both gradient and degrees from horizontal with representative lines shown for reference. Lomax model parameters A and B were jointly optimized (R_{model}, black lines on *Insets*) to fit empirical exceedances, then used to calculate P_{model} (gray lines on main figure). Smaller particles on lower, rougher (vegetated) slopes become increasingly likely to disentrain as they travel farther, leading to shorter travel distances with light-tailed distributions ($A < 0$). As particle size or slope increase, particularly on smooth (burned) surfaces, disentrainment becomes less likely with distance, allowing particles to travel farther and producing increasingly heavy-tailed distributions ($A > 0$). Note that the 0.25-gradient vegetated slope is nearly as smooth as the burned slopes (Fig. 2*A*).

could be more precisely represented through spatially and/or temporally variable Lomax parameters, $A(D(x,t), d(x,t), S(x,t), \ldots)$ and $B(D(x,t), d(x,t), S(x,t), \ldots)$, or various simplifications thereof. Spatially averaged time-dependent Lomax parameters might then better represent the evolution of mean system properties following perturbation such as wildfire or climate change, while spatially explicit time-averaged parameters might be used to capture steady-state surface variation, for example, due to downslope surface coarsening or changes in lithology. Parameters explicit in both time and space could more accurately and precisely represent the morphodynamics of evolving systems, and might be particularly relevant to problems involving short-term processes sensitive to preferential particle transport pathways, for example, when considering the impacts of postfire ravel on debris flow hazards, stream ecology, and human infrastructure.

The Light- to Heavy-Tail Transition and Energy Extraction by Surface Roughness

Previous studies (20, 60) have suggested that the angle of repose or critical hillslope angle represents a transition between light-tailed, friction-dominated transport on lower slopes, in which particles are more likely to decelerate and become trapped, and

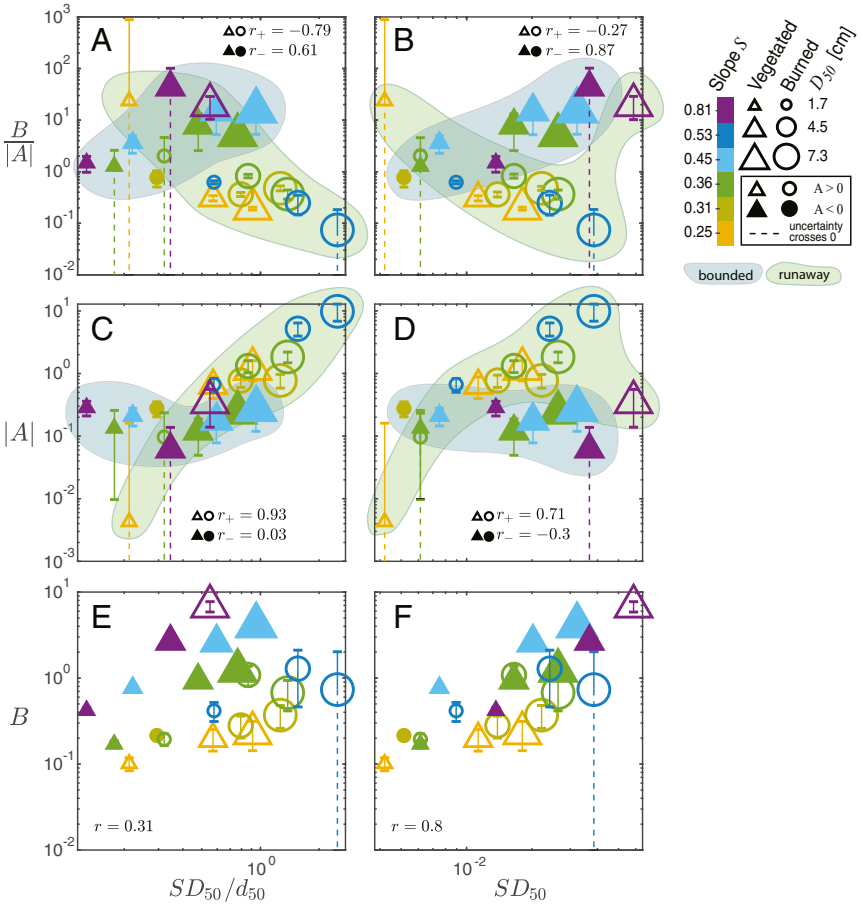

Fig. 6. Trends between the physical variables (slope S, median grain diameter D_{50}, and surface roughness d_{50}) controlling particle disentrainment and optimized Lomax model parameters. SD_{50}/d_{50} represents the ratio of energy gained from gravitational potential to energy lost to encounters with surface roughness. Group boundaries were drawn to assist with visual identification of data clusters depicting bounded ($A < 0$; blue cluster) and runaway ($A > 0$; green cluster) motion. (*A* and *B*) Characteristic distance $x = B/|A|$ increases with SD_{50}/d_{50} for negative A values (particles travel farther before motion becomes bounded over light-tailed distributions) and decreases with SD_{50}/d_{50} for positive A values (runaway motion occurs at decreasing distances over heavy-tailed distributions). Comparison of $B/|A|$ plotted against SD_{50} demonstrates that roughness appears to collapse data and account for variance in $B/|A|$. (*C* and *D*) S, D_{50}, and d_{50} all contribute to variance in Lomax shape parameter $|A|$ (shown as absolute value due to log–log axes), which controls bounded or runaway behavior and the tails of travel distance distributions. As SD_{50}/d_{50} increases, $|A|$ first decreases as negative A values approach 0 (light tails grow less light), then increases for positive A values (heavy tails grow heavier). (*E* and *F*) Conversely, S and D_{50} alone are sufficient to account for the majority of variance in scale parameter B because particle disentrainment $P \sim 1/B$ over very small travel distances where particles are less likely to encounter the full roughness distribution (Fig. 1). Bars represent 1σ uncertainty estimates (*SI Appendix*, section 4), and dashed bars indicate uncertainty extending across 0 (cut off on log–log axes).

heavy-tailed, inertia-dominated transport on steeper slopes, in which particles are more likely to accelerate. While our results are generally consistent with these findings, they demonstrate that surface roughness and grain size can substantially shift this transition point.

The onset of runaway motion reflects a transition from a regime in which frictional and collisional energy extraction approximately balances the conversion of potential to translational kinetic energy to one in which kinetic gains outpace losses. On burned slopes, our observations suggest that this transition coincides with an increasing likelihood of particle motion via tumbling and bouncing. Once particles transition from interspersed sliding and rolling with rotation primarily around the long and intermediate particle axes to rolling, tumbling, and bouncing with rotation primarily around the short particle axis (Movies S1 and S2), the lower efficiency of rotational kinetic energy extraction by collisions with the surface is unable to balance the energy gained from gravitational potential. However, while we observe the same tumbling and bouncing modes on the rougher, heavily vegetated sites, runaway motion occurs only for the largest particles on the steepest slope (Fig. 5). Instead, tumbling particles on these rough slopes experience brief regions of runaway motion stalled by collisions, evident in the "bumps" in $R(x)$ discussed previously. Hence, net motion remains bounded even on forested slopes twice as steep as the burned slopes on which runaway motion occurred (Fig. 5), demonstrating the effectiveness with which vegetative roughness is able to extract kinetic energy from mobile particles.

The process transition associated with long-runout particles was accentuated by our use of subrounded experimental particles (*SI Appendix*, section 2) which were more prone to tumbling and bouncing and enabled us to observe a range of distinctly heavy-tailed behavior in logistically manageable experimental sample sizes ($N \approx 100$ per distribution). While we expect the transition to heavy tails to occur at higher slopes for more angular particles, this experimental setup isolates the effects of slope, roughness, and grain size, revealing a fundamental mechanical control on rarefied particle motions.

Additionally, while the SD_{50}/d_{50} scaling shown in Fig. 6 is specific to the physics of rarified, ravel-type particle motion, transitions from light- to heavy-tailed behavior are known to occur in a diverse range of transport processes and settings,

including particle travel distances, travel times and velocities in hydrological contaminant and fluvial bedload transport, and rain splash transport distances (55, 61–65).

We limit our discussion to the implications of our work for rarefied, ravel-style transport processes on hillslopes, but note that the Lomax model simply provides a general framework for representing probabilistic descriptions of particle motion from light- to heavy-tailed behavior along a continuous path in parameter space controlled by physical variables—whatever those variables may be for a particular process. This framework may enable better alignment between probabilistic (e.g., ref. 44) and physics-based (e.g., refs. 20, 39, and 45) models in complex natural systems, where these two approaches can diverge. In particular, we discuss below how the particle travel distance distributions presented here relate to existing frameworks of local and nonlocal transport, as well as the implications for common hillslope formulations used to assess steady-state fluxes and evolution in geomorphic systems.

Implications of Distribution Forms and Nonlocal Transport for Naturally Occurring Processes and Landscape Evolution

As previously noted, a convolution involving volumetric particle entrainment and probability functions of travel distances provides a scale-independent description of the volumetric particle flux (44, 64). Transport that is termed local is a special case in which moments (mean, variance) of the distributions are defined. In this case, the probabilistic motion of particles at a given position can be determined completely from the properties in the immediate vicinity of that position, without convolving over other positions. However, a convolution integral is still a correct description of transport in this case. Transport that is termed nonlocal then is not a special case of transport but simply one for which a local approximation is not appropriate.

The mathematical distinction between transport characterized using local operators rather than the full convolution (i.e., a nonlocal operator; for reference, other nonlocal operators include integrals, Fourier transforms, and fractional-order derivatives) is clear-cut. Previous studies have therefore found it useful to develop separate phenomenological treatments of local versus nonlocal transport to leverage mathematical simplifications that recast these problems in terms allowing for rigorous analytical solutions (49, 50). Much of this work has centered around problems regarding tracer particles (61–63, 65–70), for which characteristic particle travel distance and rest time distributions lead to distinct particle advection and dispersion behaviors. Focusing only on travel distances, when the distribution has a light tail (i.e., moments are defined), particles disperse normally (i.e., the variance in particle position increases linearly with time) and may be described by a local advection–diffusion equation. When the distribution has a heavy tail, the particles disperse anomalously (variance increases faster than linearly with time) and must be described by nonlocal operators. Because the characteristics of light- and heavy-tailed travel distance distributions are 1) clearly stated and 2) neatly connected to the dispersion behavior, the distribution form provides an appealing distinction between "local" and "nonlocal" processes. Although nonlocal hillslope models are developed with regard to the bulk hillslope sediment flux rather than particle tracers, the same distinction between local and nonlocal transport is often applied (20, 25, 39, 49, 50, 71–74).

Our results highlight a key limitation in using this distinction to categorize the physical behavior of particles on hillslopes. Consider a series of rock drop thought experiments with a single grain size, conducted continuously along an idealized, uniformly rough and convex hillslope on which slopes approach zero at the ridge and grow increasingly steep with downslope distance. Assume that particle travel distances are light-tailed ($A < 0$) close to the ridge, or "local" by the distinction above. As we move down the hillslope, particle travel distances grow longer, and distributions approach exponential (A approaches 0). At some point, distributions transition through exponential (A crosses 0) and become heavy-tailed (A grows positive), at which point, particle motion is considered "nonlocal." As we cross this paradigm-shifting divide between "local" and "nonlocal" motion, however, the particle travel distances simply grow infinitesimally longer, exactly as they have done with each step we've taken since the ridgeline. Physically speaking, particle motion transitions smoothly and continuously, with no clear threshold or distinction between local and nonlocal behavior. As demonstrated by our data, even light-tailed distributions can have mean values long enough to surpass the physical limits of particle motion (i.e., the base of a given hillslope) (Fig. 5). These motions are still fundamentally nonlocal in origin: Particles interact with and are influenced by terrain over long distances. Thus we stress that the distinction between light- and heavy-tailed particle motion in the context of local or nonlocal transport on hillslopes is mathematical rather than physical.

We also stress that assessing the bulk hillslope sediment flux requires consideration of both particle travel distances and entrainment rates—which can also influence nonlocality. The entrainment rate describes the bulk entrainment of particles at a given position, which can vary with position along the hillslope and therefore plays a role in the flux of particles sourced from upslope. This role is evident in the influence of entrainment on steady-state hillslope profiles, where it's been shown that steady and uniform entrainment convolved with finite-mean travel distance distributions can produce steady-state hillslope profiles similar to those associated with classical local diffusive flux formulations (43). Slope-dependent entrainment convolved with the same travel distances, however, can produce profiles more similar to those resulting from nonlinear flux formulations (43, 52). These examples demonstrate the sensitivity of long-distance fluxes and their resulting profiles to the upslope (i.e., nonlocal) conditions controlling entrainment.

Hence, we argue that the physical origin of particle motion is the relevant fundamental definition of local or nonlocal motion in hillslope settings. Specifically, within the context of particle motions on hillslopes, nonlocal transport refers to the physical idea that the flux or its divergence at position x depends on factors controlling the entrainment, motion, and travel distances of particles that reach x from upslope—regardless of the form of the distribution of travel distances or entrainment. Distinct phenomenological models based on the form of the travel distance distribution may be less useful in the context of this definition, which points to the need for flux formulations able to assess fluxes of particles from all upslope distances. This brings us back to the full convolution of particle entrainment and disentrainment over upslope conditions (44). Here, the Lomax model provides a similarly phenomenological description of particle travel distances and disentrainment that is both compatible with the full convolutional flux formulation and able to account for all scales of particle motion without distinguishing between local and nonlocal behavior.

Conclusions

Some of today's most pressing geomorphic questions, for example, involving hazards or the impacts of climate change, wildfire, or land use, are concerned with short-term sediment fluxes and morphodynamics under evolving conditions. These questions are particularly relevant in steeplands, where topography undergoes frequent disturbance and adjustment. In such settings, local and steady-state approximations offer insufficient descriptions of the details of particle motion or coevolving sediment fluxes and surface attributes across scales, which could be better captured by a full nonlocal convolution (44).

For example, our results indicate that previously unexamined relationships may exist between the grain size distributions entering channel networks (53) and the topography of contributing hillslopes. This could extend the impacts of a wide range of processes known to alter surface roughness (e.g., logging, agriculture, aridification, wildfire). Preferential delivery of coarse material amplified by the increasingly frequent removal of surface roughness by wildfires (3) could also have implications for the destructive potential of postfire debris flow hazards over the coming years. Accounting for size-dependent particle travel distances could also help clarify the mechanics of downslope surface coarsening commonly observed on talus slopes (39, 56, 58) and deltas (59).

Investigating these possibilities and unraveling the feedbacks among surface topography, grain sizes, and particle motion requires the further development of nonlocal models. As mentioned above and fully explained in previous work (44, 75), the convolution of sediment entrainment with travel distance exceedances (43, 44, 52) provides a direct assessment of scale-independent (i.e., both local and nonlocal) bulk sediment fluxes inclusive of all distribution forms. In fact, this is just a specialized version of the Master equation, which is relevant to probabilistic descriptions of particle motions under both rarefied and continuum conditions from the atomic scale (76) to the galactic scale (77). Our work provides a first-order model for connecting the exceedance side of this formulation to measurable physical variables through the Lomax parameters. Future work should more deeply explore the relationship between these parameters and the physics of particle motion, toward the development of spatiotemporally explicit parameters (i.e., $A(x,t)$ and $B(x,t)$) and forward models. With similar work to develop the probabilistic representation of particle entrainment, combined with today's growing computational resources and access to high-resolution topographic data, the convolution model constitutes a profoundly powerful and flexible tool. Such a model has the potential to transform the way we predict sediment fluxes and surface evolution across scales and processes. This ability is key to building a complete understanding of sediment transport and landscape morphodynamics not only in steeplands or in response to wildfire but over all of Earth's—and perhaps other planets'—diverse surfaces.

Materials and Methods

Details on the collection, processing, and analysis of topographic data, including the calculation of roughness metric d_{50}, are available in *SI Appendix*, section 1. Experimental field site locations are reported in *SI Appendix*, Table S1. We describe the rock drop experiments in *SI Appendix*, section 2 and present experimental particle characteristics in *SI Appendix*, Table S2. We discuss the calculation of empirical travel distance distributions and disentrainment rates in *SI Appendix*, section 3. The Lomax distribution optimization and error estimation procedures are detailed in *SI Appendix*, section 4.

Data Availability. Raw lidar data used in this study are available in the UNAVCO online data archive (doi:10.7283/R3W38X). All particle travel distance data and surface-normal digital elevation model (DEM) rasters are available on GitHub (https://github.com/danicalir/Data_ParticleMotion; doi:10.5281/zenodo.3953108).

Code Availability. Matlab codes used to filter surface-normal DEMs, calculate empirical distributions, optimize Lomax parameters and reproduce all figures presented in this study are available on GitHub (https://github.com/danicalir/LomaxTools; doi: 10.5281/zenodo.3955231).

ACKNOWLEDGMENTS. We thank A. Noble and J. Noble for site access to their property; N. Candusso, B. Hunter, E. Niyangoda, J. Sayre, N. Schachtman, S. Shaw, W. Struble, and S. Wall for assistance with field experiments and data collection; K. Williams and C. Crosby for assistance with lidar data processing; G. Walton for assistance with developing the optimization algorithm; A. Wickert and A. Grubb for assistance with GitHub code and data repositories; and J. Kirchner, R. Laber, L. Sklar, J. Turowski, and D. Jerolmack for helpful discussion and suggestions. We acknowledge funding from the NSF (Award EAR-1420898 to J.J.R. and Postdoctoral Fellowship 1625311 to D.L.R.). This work includes data services provided by UNAVCO. Land access was granted by the Bureau of Land Management, with thanks to S. Post.

1. A. L. Westerling, H. G. Hidalgo, D. R. Cayan, T. W. Swetnam, Warming and earlier spring increase Western U.S. forest wildfire activity. *Science* **313**, 940–943 (2006).
2. D. R. Cayan, E. P. Maurer, M. D. Dettinger, M. Tyree, K. Hayhoe, Climate change scenarios for the California region. *Clim. Change* **87**, 21–42 (2008).
3. A. L. Westerling *et al*., Climate change and growth scenarios for California wildfire. *Clim. Change* **109**, 445–463 (2011).
4. R. A. Dibiase, M. P. Lamb, Vegetation and wildfire controls on sediment yield in bedrock landscapes. *Geophys. Res. Lett.* **40**, 1093–1097 (2013).
5. W. G. Wells, *The Effects of Fire on the Generation of Debris Flows in Southern California*, (Reviews in Engineering Geology, Geol. Soc. Am., 1987), vol. 7.
6. J. L. Florsheim, E. A. Keller, D. W. Best, Fluvial sediment transport in response to moderate storm flows following chaparral wildfire, Ventura County, southern California. *Geol. Soc. Am. Bull.* **103**, 504–511 (1991).
7. J. W. Kean, D. M. Staley, S. H. Cannon, In situ measurements of post-fire debris flows in southern California: Comparisons of the timing and magnitude of 24 debris-flow events with rainfall and soil moisture conditions. *J. Geophys. Res. Earth Surf.* **116**, F04019 (2011).
8. J. W. Kean, S. W. McCoy, G. E. Tucker, D. M. Staley, J. A. Coe, Runoff-generated debris flows: Observations and modeling of surge initiation, magnitude, and frequency. *J. Geophys. Res. Earth Surf.* **118**, 2190–2207 (2013).
9. R. A. DiBiase, M. P. Lamb, Dry sediment loading of headwater channels fuels post-wildfire debris flows in bedrock landscapes. *Geology* **48**, 189–193 (2020).
10. M. P. Lamb, J. S. Scheingross, W. H. Amidon, E. Swanson, A. Limaye, A model for fire-induced sediment yield by dry ravel in steep landscapes. *J. Geophys. Res.* **116**, F03006 (2011).
11. M. P. Lamb, M. Levina, R. A. DiBiase, B. M. Fuller, Sediment storage by vegetation in steep bedrock landscapes: Theory, experiments, and implications for postfire sediment yield. *J. Geophys. Res. Earth Surf.* **118**, 1147–1160 (2013).
12. J. J. Roering, M. Gerber, Fire and the evolution of steep, soil-mantled landscapes. *Geology* **33**, 349–352 (2005).
13. E. J. Gabet, Sediment transport by dry ravel. *J. Geophys. Res. Solid Earth* **108**, 2049 (2003).
14. R. A. Shakesby, S. H. Doerr, Wildfire as a hydrological and geomorphological agent. *Earth Sci. Rev.* **74**, 269–307 (2006).
15. K. A. Bennett, "Effects of slash burning on surface soil erosion rates in the Oregon Coast Range," MSc thesis, Oregon State University, Corvallis, OR (1982).
16. F. J. Swanson, "Fire and geomorphic processes" in *Fire Regimes and Ecosystem Properties: Proceedings of the Conference*, H. A. Mooney, Ed. (US Forest Service, 1981), pp. 401–420.
17. M. Jackson, J. J. Roering, Post-fire geomorphic response in steep, forested landscapes: Oregon coast range, USA. *Quat. Sci. Rev.* **28**, 1131–1146 (2009).
18. J. Lavé, D. Burbank, Denudation processes and rates in the Transverse Ranges, southern California: Erosional response of a transitional landscape to external and anthropogenic forcing. *J. Geophys. Res. Earth Surf.* **109**, F000023 (2004).
19. X. Fu, "A physical model of dry ravel movement, MS thesis, Washington State University, Pullman, WA (2004).
20. E. J. Gabet, M. K. Mendoza, Particle transport over rough hillslope surfaces by dry ravel: Experiments and simulations with implications for nonlocal sediment flux. *J. Geophys. Res. Earth Surf.* **117**, F01019 (2012).
21. M. E. Miller, W. J. Elliot, M. Billmire, P. R. Robichaud, K. A. Endsley, Rapid-response tools and datasets for post-fire remediation: Linking remote sensing and process-based hydrological models. *Int. J. Wildland Fire* **25**, 1061–1073 (2016).
22. W. E. H. Culling, Soil creep and the development of hillside slopes. *J. Geol.* **71**, 127–161 (1963).
23. J. J. Roering, J. W. Kirchner, W. E. Dietrich, Evidence for nonlinear, diffusive sediment transport on hillslopes and implications for landscape morphology. *Water Resour. Res.* **35**, 853–870 (1999).
24. W. E. Dietrich *et al*., Geomorphic transport laws for predicting landscape form and dynamics. *Geophys. Monogr. Ser.* **135**, 103–132 (2003).
25. G. E. Tucker, D. N. Bradley, Trouble with diffusion: Reassessing hillslope erosion laws with a particle-based model. *J. Geophys. Res.* **115**, F00A10 (2010).
26. N. S. Deshpande, D. J. Furbish, P. E. Arratia, D. J. Jerolmack, The perpetual fragility of creeping hillslopes. EarthArXiv:10.31223.osf.io/qc9jh (18 May 2020).
27. B. Ferdowsi, C. P. Ortiz, D. J. Jerolmack, Glassy dynamics of landscape evolution. *Proc. Natl. Acad. Sci. U.S.A.* **115**, 4827–4832 (2018).
28. M. Houssais, D. J. Jerolmack, Toward a unifying constitutive relation for sediment transport across environments. *Geomorphology* **277**, 251–264 (2017).
29. E. J. Gabet, T. Dunne, Sediment detachment by rain power. *Water Resour. Res.* **39**, 1002 (2003).
30. D. J. Furbish, K. K. Hamner, M. W. Schmeeckle, M. N. Borosund, S. M. Mudd, Rain splash of dry sand revealed by high-speed imaging and sticky paper splash targets. *J. Geophys. Res.* **112**, F01001 (2007).

31. D. J. Furbish, E. M. Childs, P. K. Haff, M. W. Schmeeckle, Rain splash of soil grains as a stochastic advection-dispersion process, with implications for desert plant-soil interactions and land-surface evolution. *J. Geophys. Res. Solid Earth* **114**, F00A03 (2009).
32. T. Dunne, D. V. Malmon, S. M. Mudd, A rain splash transport equation assimilating field and laboratory measurements. *J. Geophys. Res.* **115**, F01001 (2010).
33. R. S. Anderson, Modeling the tor-dotted crests, bedrock edges, and parabolic profiles of high alpine surfaces of the Wind River Range, Wyoming. *Geomorphology* **46**, 35–58 (2002).
34. M. J. Kirkby, Measurement and theory of soil creep. *J. Geol.* **75**, 359–378 (1967).
35. E. J. Gabet, O. J. Reichman, E. W. Seabloom, The effects of bioturbation on soil processes and sediment transport. *Annu. Rev. Earth Planet. Sci.* **31**, 249–273 (2003).
36. K. Kamrin, G. Koval, Nonlocal constitutive relation for steady granular flow. *Phys. Rev. Lett.* **108**, 178301 (2012).
37. D. L. Henann, K. Kamrin, Continuum thermomechanics of the nonlocal granular rheology. *Int. J. Plast.* **60**, 145–162 (2014).
38. F. Bourrier, F. Berger, P. Tardif, L. Dorren, O. Hungr, Rockfall rebound: Comparison of detailed field experiments and alternative modelling approaches. *Earth Surf. Process. Landf.* **37**, 656–665 (2012).
39. R. A. DiBiase, M. P. Lamb, V. Ganti, A. M. Booth, Slope, grain size, and roughness controls on dry sediment transport and storage on steep hillslopes. *J. Geophys. Res. Earth Surf.* **122**, 941–960 (2017).
40. S. A. Norman, R. J. Schaetzl, T. W. Small, Effects of slope angle on mass movement by tree uprooting. *Geomorphology* **14**, 19–27 (1995).
41. E. J. Gabet, Gopher bioturbation: Field evidence for non-linear hillslope diffusion. *Earth Surf. Process. Landf.* **25**, 1419–1428 (2000).
42. R. A. Dibiase, A. M. Heimsath, K. X. Whipple, Hillslope response to tectonic forcing in threshold landscapes. *Earth Surf. Process. Landf.* **37**, 855–865 (2012).
43. D. J. Furbish, P. K. Haff, From divots to swales: Hillslope sediment transport across diverse length scales. *J. Geophys. Res.* **115**, F03001 (2010).
44. D. J. Furbish, J. J. Roering, Sediment disentrainment and the concept of local versus nonlocal transport on hillslopes. *J. Geophys. Res. Earth Surf.* **118**, 937–952 (2013).
45. M. J. Kirkby, I. Statham, Surface stone movement and scree formation. *J. Geol.* **83**, 349–362 (1975).
46. J. J. Roering, Soil creep and convex-upward velocity profiles: Theoretical and experimental investigation of disturbance-driven sediment transport on hillslopes. *Earth Surf. Process. Landf.* **29**, 1597–1612 (2004).
47. D. J. Furbish, P. K. Haff, W. E. Dietrich, A. M. Heimsath, Statistical description of slope-dependent soil transport and the diffusion-like coefficient. *J. Geophys. Res.* **114**, F00A05 (2009).
48. F. Bourrier, N. Eckert, F. Nicot, F. Darve, Bayesian stochastic modeling of a spherical rock bouncing on a coarse soil. *Nat. Hazards Earth Syst. Sci.* **9**, 831–846 (2009).
49. R. Schumer, M. M. Meerschaert, B. Baeumer, Fractional advection-dispersion equations for modeling transport at the Earth surface. *J. Geophys. Res.* **114**, F00A07 (2009).
50. E. Foufoula-Georgiou, V. Ganti, W. E. Dietrich, A nonlocal theory of sediment transport on hillslopes. *J. Geophys. Res. Earth Surf.* **115**, F00A16 (2010).
51. T. H. Doane, D. L. Roth, J. J. Roering, D. J. Furbish, Compression and decay of hillslope topographic variance in Fourier wavenumber domain. *J. Geophys. Res. Earth Surf.* **124**, 60–79 (2019).
52. T. H. Doane, D. J. Furbish, J. J. Roering, R. Schumer, D. J. Morgan, Nonlocal sediment transport on steep lateral moraines, eastern sierra Nevada, California, USA. *J. Geophys. Res. Earth Surf.* **123**, 187–208 (2018).
53. L. S. Sklar *et al*., The problem of predicting the size distribution of sediment supplied by hillslopes to rivers. *Geomorphology* **277**, 31–49 (2017).
54. L. M. Perreault, E. M. Yager, R. Aalto, Effects of gradient, distance, curvature and aspect on steep burned and unburned hillslope soil erosion and deposition. *Earth Surf. Process. Landf.* **42**, 1033–1048 (2017).
55. A. Ghahramani, I. Yoshiharu, S. M. Mudd, Field experiments constraining the probability distribution of particle travel distances during natural rainstorms on different slope gradients. *Earth Surf. Process. Landf.* **37**, 473–485 (2012).
56. I. Statham, A scree slope rockfall model. *Earth Surf. Process. Landf.* **1**, 43–62 (1976).
57. R. L. Wasserstein, A. L. Schirm, N. A. Lazar, Moving to a world beyond "p < 0.05.". *Am. Stat.* **73**, 1–19 (2019).
58. D. Ventra, G. C. Dìaz, P. L. De Boer, Colluvial sedimentation in a hyperarid setting (Atacama Desert, northern Chile): Geomorphic controls and stratigraphic facies variability. *Sedimentology* **60**, 1257–1290 (2013).
59. W. Nemec, "Aspects of sediment movement on steep delta slopes" in *Coarse-Grained Deltas*, A. Colella, D. B. Prior, Eds. (Blackwell, 1990), pp. 29–73.
60. F.-X. Riguidel, R. Jullien, G. H. Ristow, A. Hansen, D. Bideau, Behaviour of a sphere on a rough inclined plane. *J. Phys. I* **4**, 261–272 (1994).
61. V. Ganti, M. M. Meerschaert, E. Foufoula-Georgiou, E. Viparelli, G. Parker, Normal and anomalous diffusion of gravel tracer particles in rivers. *J. Geophys. Res. Earth Surf.* **115**, F00A12 (2010).
62. T. C. Ashley, R. C. Mahon, S. Naqshband, K. C. Leary, B. McElroy, Probability distributions of particle hop distance and travel time over equilibrium mobile bedforms. *J. Geophys. Res. Earth Surf.* **125** e2020JF005647 (2020).
63. D. A. Benson, R. Schumer, M. M. Meerschaert, S. W. Wheatcraft, Fractional dispersion, Lévy motion, and the MADE tracer tests. *Transp. Porous Media* **42**, 211–240 (2001).
64. A. Pelosi, G. Parker, R. Schumer, H.-B. Ma, Exner-based master equation for transport and dispersion of river pebble tracers: Derivation, asymptotic forms, and quantification of nonlocal vertical dispersion. *J. Geophys. Res. Earth Surf.* **119**, 1818–1832 (2014).
65. D. N. Bradley, G. E. Tucker, D. A. Benson, Fractional dispersion in a sand bed river. *J. Geophys. Res.* **115**, F00A09 (2010).
66. B. Berkowitz, A. Cortis, M. Dentz, H. Scher, Modeling Non-fickian transport in geological formations as a continuous time random walk. *Rev. Geophys.* **44**, RG2003 (2006).
67. J. W. Kirchner, X. Feng, C. Neal, Fractal stream chemistry and its implications for contaminant transport in catchments. *Nature* **403**, 524–527 (2000).
68. V. Nikora, H. Habersack, T. Huber, I. McEwan, On bed particle diffusion in gravel bed flows under weak bed load transport. *Water Resour. Res.* **38**, 1081 (2002).
69. E. R. Weeks, H. L. Swinney, Anomalous diffusion resulting from strongly asymmetric random walks. *Phys. Rev. E Stat. Phys. Plasmas Fluids Relat. Interdiscip. Topics* **57**, 4915–4920 (1998).
70. Z. Q. Deng, J. L. M. P. De Lima, M. I. P. De Lima, V. P. Singh, A fractional dispersion model for overland solute transport. *Water Resour. Res.* **42**, W03416 (2006).
71. C. P. Stark, E. Foufoula-Georgiou, V. Ganti, A nonlocal theory of sediment buffering and bedrock channel evolution. *J. Geophys. Res. Earth Surf.* **114**, H33K06 (2009).
72. V. R. Voller, C. Paola, Can anomalous diffusion describe depositional fluvial profiles? *J. Geophys. Res. Earth Surf.* **115**, F00A13 (2010).
73. F. Falcini, E. Foufoula-Georgiou, V. Ganti, C. Paola, V. R. Voller, A combined nonlinear and nonlocal model for topographic evolution in channelized depositional systems. *J. Geophys. Res. Earth Surf.* **118**, 1617–1627 (2013).
74. V. R. Voller, V. Ganti, C. Paola, E. Foufoula-Georgiou, Does the flow of information in a landscape have direction? *Geophys. Res. Lett.* **39**, L01403 (2012).
75. D. J. Furbish, S. L. Fathel, M. W. Schmeeckle, D. J. Jerolmack, R. Schumer, The elements and richness of particle diffusion during sediment transport at small timescales. *Earth Surf. Process. Landf.* **42**, 214–237 (2017).
76. A. Einstein, On the movement of small particles suspended in stationary liquids required by the molecular-kinetic theory of heat. *Ann. Phys.* **17**, 549–560 (1905).
77. S. Chandrasekhar, Stochastic problems in physics and astronomy. *Rev. Mod. Phys.* **15**, 1–89 (1943).